Journal of Magnetic Resonance **155,** 100–105 (2002)
doi:10.1006/jmre.2002.2509, available online at http://www.idealibrary.com on IDEAL®

Determination of Hyperfine Tensor Components from Nuclear Frequencies at Canonical Orientations of the *g*-Tensor

Alexander A. Shubin* and Sergei A. Dikanov†

*Boreskov Institute of Catalysis, Russian Academy of Sciences, Novosibirsk 630090, Russia; and †Illinois EPR Research Center and Department of Veterinary Clinical Medicine, University of Illinois at Urbana–Champaign, Urbana, Illinois 61801 and Institute of Chemical Kinetics and Combustion, Russian Academy of Sciences, Novosibirsk 630090, Russia

Received September 7, 2001; revised January 28, 2002

The analytical procedure for the determination of all components of the symmetric hyperfine tensor of the $I = 1/2$ nucleus in the *g*-tensor coordinate system is described, assuming that nuclear frequencies corresponding to the principal directions of the *g*-tensor and exact values of the external magnetic field (or nuclear Zeeman frequencies) are experimentally available.

Key Words: ***g*-tensor; canonical orientations; orientation-selected ENDOR/ESEEM spectra; nuclear frequencies; components of hyperfine tensor.**

INTRODUCTION

Structural studies of paramagnetic metal complexes or radicals in frozen solutions or powders by high-resolution EPR spectroscopy, including CW and pulsed ENDOR and one- and two-dimensional ESEEM, are based on the measurement of hyperfine and quadrupole couplings from magnetic nuclei in their surroundings (*1–5*). The most complete characterization of electron–nucleus interactions would require determination of the principal values of hyperfine and quadrupole (for nuclei with $I \geq 1$) tensors and the orientation of their principal directions relative to the *g*-tensor axes.

In this study we consider the special case of paramagnetic species, which posses EPR spectra with the lineshapes determined by the rhombic *g*-tensor anisotropy ($g_1 > g_2 > g_3$) without resolved hyperfine structure. The orientation-selected ENDOR or ESEEM experiments are usually done to determine the nuclear frequencies at different points along the complete EPR spectrum (*6*). These experiments select species with different orientations of the *g*-tensor relative to the applied magnetic field. For instance, the measurements with the field chosen to select the low and high extreme edges near the maximal and minimal *g*-values give "single-crystal-like" patterns from the species whose g_1 and g_3 axes are directed along the magnetic field. It is generally accepted and supported by a large body of experimental data that nuclei with $I = 1/2$ (such as ^{1}H, ^{13}C, ^{15}N, ^{19}F, and ^{31}P) produce a doublet of lines with splittings equal to the corresponding diagonal element of the hyperfine tensor in both single-crystal-like spectra (*7–9*).

In contrast, the resonance condition at the intermediate g_2 value is fulfilled by many different yet well-defined orientations. The lineshapes of nuclear frequencies measured at the g_2 position are more complex. However, Hoffman *et al*. formulated rules for accurate estimation of the hyperfine splitting along the g_2 direction itself (*7*). Thus, measurements at three points corresponding to the singularities of the rhombic EPR spectrum provide diagonal elements of the hyperfine tensor, which also determine an isotropic hyperfine constant. For many ENDOR/ESEEM spectroscopic studies this approach represents the end point, because the complete determination of the tensor, even for the simplest case of one $I = 1/2$ nucleus, would require a much more extended effort, based on numerous simulations of the complete set of orientation-selected spectra collected over the entire EPR spectrum (*8–10*). The complexity of the analysis would increase proportionally if the tensors of several nuclei need to be determined from experimental spectra of nuclear frequencies.

In the present article we describe a simple analytical procedure for the determination of *all* components of *symmetric* hyperfine tensor of $I = 1/2$ nucleus in the *g*-tensor coordinate system when *g*-tensor anisotropy dominates all other interactions. It is assumed that nuclear frequencies corresponding to the principal directions of the *g*-tensor and exact values of the external magnetic field (or nuclear Zeeman frequencies) are experimentally available. This procedure works best when the hyperfine interaction is comparable with the nuclear Zeeman interaction. We anticipate that this approach will provide an accurate, rapid estimate of hyperfine tensors and will simplify the subsequent simulation procedure of orientation-selected ENDOR/ESEEM spectra. It can be applied not only in the case of a single nucleus but also when the spectra are contributed by several nuclei.

One caveat is necessary. It is known that for low-symmetry systems, the hyperfine tensor is, in general, asymmetric (*11–15*). Hyperfine tensor asymmetry has been treated experimentally by several authors (see (*14, 15*) and references therein). Nevertheless, for species with $S = 1/2$ this asymmetry is often small and does not exceed a few percent. Therefore, the assumption of a symmetric hyperfine tensor is appropriate in most cases

1090-7807/02 $35.00

and is widely used in the interpretation of experimental EPR or ENDOR data, in theoretical estimates, and in *ab initio* quantum-chemical calculations.

THEORY

The spin Hamiltonian describing the interaction of electron spin $S = 1/2$ with a nucleus $I = 1/2$ in a magnetic field $\vec{H} = H\vec{n}$ ($\vec{n}$ is the unity vector in a magnetic field direction) has the form

$$\hat{\mathcal{H}} = \beta H(\vec{n} \cdot \boldsymbol{g} \cdot \hat{\vec{S}}) + h(\hat{\vec{S}} \cdot \boldsymbol{A} \cdot \hat{\vec{I}}) - g_I \beta_I H(\vec{n} \cdot \hat{\vec{I}}). \quad [1]$$

Using the nuclear Zeeman interaction of the form presented in [1], we restrict our consideration to spin systems where the pseudo-Zeeman effect is negligible, so that no low-lying excited states coupled to the ground state are present. The vector that determines the direction of the electron spin quantization axis may be written as

$$\vec{\xi} = \frac{\vec{n} \cdot \boldsymbol{g}}{g_{ef}}, \quad [2]$$

where

$$g_{ef} = (\vec{n} \cdot \boldsymbol{g} \cdot \tilde{\boldsymbol{g}} \cdot \vec{n})^{1/2} \quad [3]$$

and $\tilde{\boldsymbol{g}}$ designates the transposed g-tensor. Then, in the first order of perturbation theory, the effective nuclear spin-Hamiltonian $\hat{\mathcal{H}}_{\mathcal{I}}$ corresponding to $\hat{\mathcal{H}}$ from Eq. [1] is equal to

$$\hat{\mathcal{H}}_{\mathcal{I}} = m_S h(\vec{\xi} \cdot \boldsymbol{A} \cdot \hat{\vec{I}}) - h\nu_I(\vec{n} \cdot \hat{\vec{I}}) \quad [4]$$

or

$$\hat{\mathcal{H}}_{\mathcal{I}} = \left(\vec{b}_{\alpha(\beta)} \cdot \hat{\vec{I}}\right) \quad [5]$$

with

$$\vec{b}_{\alpha(\beta)} = m_S h\vec{\xi} \cdot \boldsymbol{A} - h\nu_I\vec{n} \quad [6a]$$

$$\nu_I = \frac{g_I \beta_I H}{h} \quad [6b]$$

for $m_S = \pm\frac{1}{2}$, respectively.

The effective nuclear spin-Hamiltonian [4] has the eigenvalues

$$E_m(m_I) = m_I \cdot \left|\vec{b}_{\alpha(\beta)}\right|, \quad [7]$$

where $m_I = -I, -I+1, \ldots, +I$ are projections of the nuclear spin I on the $\vec{b}_{\alpha(\beta)}$ directions. This determines the frequencies of nuclear transition with $|\Delta m_I| = 1$ as

$$\nu_{\alpha(\beta)} = \frac{\left|\vec{b}_{\alpha(\beta)}\right|}{h}. \quad [8]$$

From Eqs. [6] and [8] this leads to

$$\nu^2_{\alpha(\beta)} = \nu_I^2 + m_S^2(\vec{\xi} \cdot \boldsymbol{A} \cdot \tilde{\boldsymbol{A}} \cdot \vec{\xi}) - 2m_S\nu_I(\vec{\xi} \cdot \boldsymbol{A} \cdot \vec{n}). \quad [9]$$

Writing Eq. [9] in explicit form for ν_α and ν_β, one finds that

$$2\left(\nu_\alpha^2 + \nu_\beta^2 - 2\nu_I^2\right) = (\vec{\xi} \cdot \boldsymbol{A} \cdot \tilde{\boldsymbol{A}} \cdot \vec{\xi}) \quad [10]$$

and

$$\nu_\beta^2 - \nu_\alpha^2 = 2\nu_I(\vec{\xi} \cdot \boldsymbol{A} \cdot \vec{n}). \quad [11]$$

For orientation-selected experiments performed at constant microwave frequency, ν_I in Eqs. [9]–[11] is not constant and depends on the choice of the g-value. In addition to the above-mentioned symmetric approximation for the $\boldsymbol{A}$ tensor it is general practice to use the assumption of a symmetric g-tensor in the analysis of ENDOR lineshapes of powder and glassy samples. In this situation, if the magnetic field coincides with one of the principal directions $\vec{e}_j$ of the g-tensor (that is, $\vec{n} = \vec{e}_j$), then $\vec{\xi} = \vec{e}_j$ and

$$g_{ef,j} = g_j = (\vec{e}_j \cdot \boldsymbol{g} \cdot \vec{e}_j) = (\vec{e}_j \cdot \boldsymbol{g}^2 \cdot \vec{e}_j)^{1/2}. \quad [12]$$

Equations [10] and [11] are transformed to

$$A_{jj} = (\vec{e}_j \cdot \boldsymbol{A} \cdot \vec{e}_j) = \frac{1}{2\nu_I}\left(\nu_\beta^2 - \nu_\alpha^2\right) \quad [13]$$

$$(A^2)_{jj} = (\vec{e}_j \cdot \boldsymbol{A}^2 \cdot \vec{e}_j) = 2\left(\nu_\alpha^2 + \nu_\beta^2 - 2\nu_I^2\right). \quad [14]$$

Thus, the nuclear frequencies along the principal directions $\vec{e}_j$ of g-tensor provide the diagonal elements of $\boldsymbol{A}$ and $\boldsymbol{A}^2$ tensors. However, because the $\boldsymbol{A}$ tensor *is by implication symmetric,* knowledge of the diagonal elements of $\boldsymbol{A}$ and $\boldsymbol{A}^2$ opens the way to determination of the *absolute values* of the nondiagonal components of the $\boldsymbol{A}$ tensor as well. According to the definition of the symmetric $\boldsymbol{A}$ tensor

$$(A^2)_{xx} = (A_{xx})^2 + (A_{xy})^2 + (A_{xz})^2 \quad [15a]$$

$$(A^2)_{yy} = (A_{yy})^2 + (A_{xy})^2 + (A_{yz})^2 \quad [15b]$$

$$(A^2)_{zz} = (A_{zz})^2 + (A_{xz})^2 + (A_{yz})^2. \quad [15c]$$

Subtracting [15c] from the sum of [15a] and [15b], one can get the nondiagonal A_{xy} element of the hyperfine tensor in the

g-tensor coordinate system,

$$(A_{xy})^2 = \frac{1}{2}\{[(A^2)_{xx} - (A_{xx})^2] + [(A^2)_{yy} - (A_{yy})^2] - [(A^2)_{zz} - (A_{zz})^2]\} \quad [16a]$$

In a similar way one can find that

$$(A_{xz})^2 = \frac{1}{2}\{[(A^2)_{xx} - (A_{xx})^2] - [(A^2)_{yy} - (A_{yy})^2] + [(A^2)_{zz} - (A_{zz})^2]\} \quad [16b]$$

$$(A_{yz})^2 = \frac{1}{2}\{-[(A^2)_{xx} - (A_{xx})^2] + [(A^2)_{yy} - (A_{yy})^2] + [(A^2)_{zz} - (A_{zz})^2]\}. \quad [16c]$$

From Eqs. [13], [14], and [16], the complete hyperfine tensor in the g-tensor coordinate system can be derived. If necessary, the standard procedure of tensor diagonalization can be applied now to determine the principal values of the $\boldsymbol{A}$ tensor and the orientation of its principal directions relative to the principal g-tensor axes.

DISCUSSION

The formal procedure described for determination of the elements of the $\boldsymbol{A}$ matrix includes several uncertainties associated with the signs of the tensor elements. The absolute signs of hyperfine tensors are undetermined in EPR and its extensions. The sign of tensor $\boldsymbol{A}$ influences the frequencies of ν_α and ν_β via the last linear term in Eq. [9] and a change of the sign for $\boldsymbol{A}$ and m_S does not alter this equation. The arbitrary assignment of two experimental frequencies to ν_α and ν_β leads to an undefined sign for each A_{jj} element and, therefore, only the relative signs of different components can be considered. This makes it possible to choose element A_{xx} as positive, for example. As a result, there are four different combinations of relative signs for the diagonal elements A_{xx}, A_{yy}, and A_{zz}, i.e., $(+++)$, $(++-)$, $(+-+)$, $(+--)$ and, respectively, four different values of isotropic hyperfine couplings $a_{iso} = 1/3\ Tr(\boldsymbol{A})$, in addition to the above-mentioned possibility of sign inversion for all elements of the $\boldsymbol{A}$ tensor.

There is also some sign uncertainty in the determination of nondiagonal elements of the $\boldsymbol{A}$ tensor, because nuclear frequencies in canonical orientations of g-tensor do not depend on these signs. It may be easily demonstrated from a detailed analysis of the angular dependence of $\nu_{\alpha,\beta}$ in noncanonical orientations that four choices for A_{xy}, A_{xz}, and A_{yz} signs,

$$(A_{xy}, A_{xz}, A_{yz}), \quad (-A_{xy}, -A_{xz}, A_{yz}), \quad (-A_{xy}, A_{xz}, -A_{yz}), \quad (A_{xy}, -A_{xz}, -A_{yz}), \quad [17]$$

lead to the same ENDOR/ESEEM *powder* pattern. In fact, the last three combinations in Eq. [17] correspond to rotations of the $\boldsymbol{A}$ tensor around the three different principal axes of the g-tensor by π. This allows one to examine *only two* (instead of eight) possible sets of nondiagonal elements of the $\boldsymbol{A}$ tensor:

$$(|A_{xy}|, |A_{xz}|, |A_{yz}|) \quad \text{and} \quad (-|A_{xy}|, -|A_{xz}|, -|A_{yz}|). \quad [18]$$

We anticipate that subsequent, more definite, assignment of the relative signs of the $\boldsymbol{A}$ tensor elements could be performed by complete simulation of orientation-selected ENDOR/ESEEM patterns including noncanonical orientations. Information from other sources such as quantum-chemical calculations or comparison with experimentally known similar systems may also be used for both relative and absolute sign assignment. For example, the choice of absolute sign can be performed after the diagonalization of the tensor and additional quantum-chemical analysis of the mechanism of hyperfine interaction between electron and nucleus in each case.

We illustrate the proposed approach for determination of the hyperfine tensor components exploring simulated orientation-selected ENDOR spectra for paramagnetic species $S = 1/2$ with $g_1, g_2, g_3 = 1.9, 1.95, 2.1$. ^{13}C ENDOR spectra in the Q-band (35 GHz) at g_1, g_2, g_3 were simulated for two sets of parameters, $A_1, A_2, A_3 = -0.5, 2, 4$ MHz; $\alpha, \beta, \gamma = 40, 60, 20^\circ$ (**I**) and $A_1, A_2, A_3 = -6, 2, 8$ MHz; $\alpha, \beta, \gamma = 30, 60, 165^\circ$ (**II**), using the GENDOR program (2, 7, 8, 16). Details of the simulation are given in the legend to Fig. 1. The difference

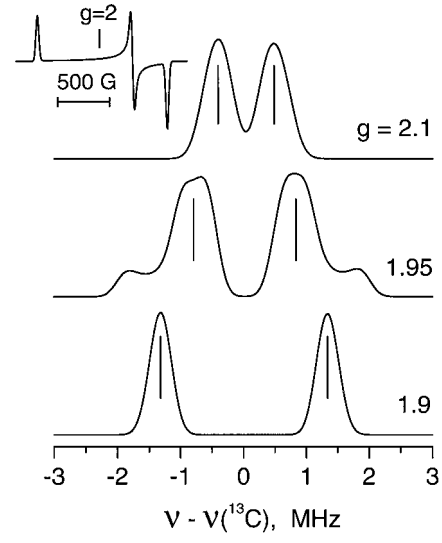

FIG. 1. ^{13}C ENDOR spectra (35 GHz) simulated at canonical orientations of the g-tensor for the $S = 1/2, I = 1/2$ system with $g_1 = 1.9, g_2 = 1.95, g_3 = 2.1$, and $A_1 = -0.5$ MHz, $A_2 = 2$ MHz, $A_3 = 4$ MHz. Euler angles describing orientation of the hyperfine tensor relative to the g-tensor are as follows: $\alpha = 40^\circ, \beta = 60^\circ, \gamma = 20^\circ$. The linewidth of individual ENDOR features was taken as 0.2 MHz, and EPR linewidth was taken as 20 G. The corresponding powder EPR spectrum is shown in the upper inset. Vertical lines mark "experimental" ν_α and ν_β nuclear frequencies used for subsequent calculations.

between the two sets is that the hyperfine interaction is much smaller then ^{13}C nuclear Zeeman for set **I**, whereas these interactions may be considered as comparable for set **II** (ν_I is equal to 14.09, 13.729, and 12.748 MHz for observation at g_1, g_2, g_3, respectively). The "experimental" nuclear frequency (ν_α or ν_β) (Figs. 1 and 3) was determined from the midpoint of the width of the corresponding ENDOR peak at half height. The lower frequency peak was assigned to ν_α in all cases (although this is somewhat arbitrary for set **II** and ENDOR observation at g_3).

The exact matrix of the hyperfine tensor in the g-tensor coordinate system for set **I** is equal to

$$\boldsymbol{A}_{exact} = \begin{pmatrix} 2.831 & 0.541 & 0.948 \\ 0.541 & 1.824 & 1.704 \\ 0.948 & 1.704 & 0.844 \end{pmatrix} \text{MHz}.$$

It is convenient to define $\Delta_\alpha = \nu_\alpha - \nu_I$, $\Delta_\beta = \nu_\beta - \nu_I$ and rewrite Eqs. [13], [14] in the form more suitable for practical applications:

$$A_{jj} = (\Delta_\beta - \Delta_\alpha)\left(1 + \frac{\Delta_\alpha + \Delta_\beta}{2\nu_I}\right) \quad [19]$$

$$(A^2)_{jj} = 2\left[2\nu_I(\Delta_\alpha + \Delta_\beta) + \Delta_\alpha^2 + \Delta_\beta^2\right]. \quad [20]$$

Calculation for the set **I** gives values for $\Delta_{\alpha,exact} = -1.404$, -0.881, -0.384 MHz and $\Delta_{\beta,exact} = 1.425, 0.940, 0.458$ MHz for g_1, g_2, g_3, respectively. The "experimental" values for these parameters found from the calculated spectra of Fig. 1 are as follows: $\Delta_{\alpha,found} = -1.319, -0.793, -0.405$ MHz; $\Delta_{\beta,found} = 1.339, 0.833, 0.486$ MHz. These give with Eqs. [16], [19], [20]

$$\boldsymbol{A}_{found} = \begin{pmatrix} 2.66 & 0 & 1.243 \\ 0 & 1.628 & 1.611 \\ 1.243 & 1.611 & 0.894 \end{pmatrix} \text{MHz}.$$

In the above matrix we forced $A_{xy} = A_{yx} = 0$ because otherwise the insufficient precision in the frequency measurements from the spectra leads to the senseless result of a negative square, $(A_{xy})^2 = -0.411$ MHz^2 from Eq. [16a]. On the other hand, in this case there is no influence of the sign of the nondiagonal elements of the hyperfine tensor (see Eqs. [17, 18]) on its principal values, A_1, A_2, and A_3. The principal values and Euler angles found for four possible choices of relative signs of hyperfine tensor diagonal elements are collected in Table 1 while the corresponding ENDOR spectra at g_1, g_2, g_3 are shown in Fig. 2. It is quite evident from comparison of the spectra at g_2 with the corresponding spectrum in Fig. 1 that the choice $(+++)$ of the signs of A_{xx}, A_{yy}, and A_{zz} elements provides the best fit and gives the principal values and Euler angles (Table 1) closest to their exact values.

TABLE 1

Different Sets of Hyperfine Interaction Parameters Determined from Spectra (Fig. 1) Simulated with $A_1 = -0.5$ MHz, $A_2 = 2$ MHz, $A_3 = 4$ MHz, $\alpha = 40°, \beta = 60°, \gamma = 20°$

The sign of A_{xx}, A_{yy}, and A_{zz}	A_1, MHz	A_2, MHz	A_3, MHz	α, ○	β, ○	γ, ○
$(+++)$	−0.69	2.19	3.68	32.7	55.4	17.6
$(+-+)$	−2.47	0.97	3.43	11.1	58.8	57.3
$(++-)$	−1.95	2.09	3.26	25.5	66.4	14.9
$(+--)$	−3.02	0.05	3.11	6.98	70.3	46.5

The corresponding exact characteristics calculated for set **II** are equal to

$$\boldsymbol{A}_{exact} = \begin{pmatrix} 2.975 & 1.873 & 5.915 \\ 1.873 & 3.123 & 1.415 \\ 5.915 & 1.415 & -2.098 \end{pmatrix} \text{MHz},$$

$\Delta_{\alpha,exact} = -1.112, -1.505, 1.380$ MHz, and $\Delta_{\beta,exact} = 1.794$, $1.606, -0.660$ MHz for g_1, g_2, g_3, respectively. ENDOR spectra (Fig. 3) calculated with set **II** give $\Delta_{\alpha,found} = -1.074$, $-1.272, -0.656$ MHz, $\Delta_{\beta,found} = 1.677, 1.417, 1.439$ MHz, which lead to

$$\boldsymbol{A}_{found} = \begin{pmatrix} 2.81 & 0.915 & 5.758 \\ 0.915 & 2.704 & 2.665 \\ 5.758 & 2.665 & 2.159 \end{pmatrix} \text{MHz}.$$

Table 2 contains principal values and Euler angles for eight possible choices of relative signs of hyperfine tensor elements. Corresponded simulated ENDOR spectra are shown in Figs. 4

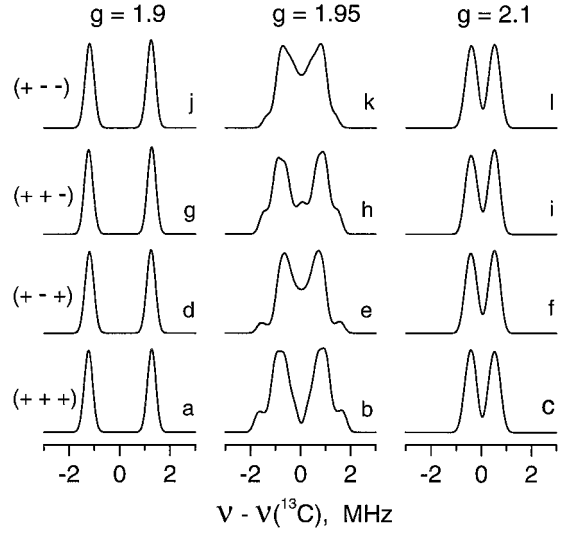

FIG. 2. ^{13}C ENDOR spectra (35 GHz) simulated using hyperfine tensor parameters presented in Table 1. All linewidths are the same as in Fig. 1.

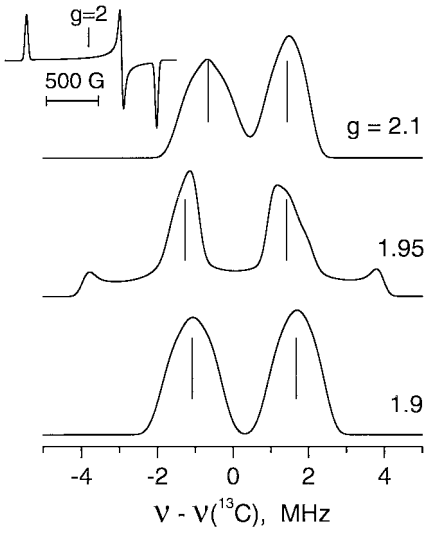

FIG. 3. The same as Fig. 1 except $A_1 = -6$ MHz, $A_2 = 2$ MHz, $A_3 = 8$ MHz, $\alpha = 30°$, $\beta = 60°$, $\gamma = 165°$.

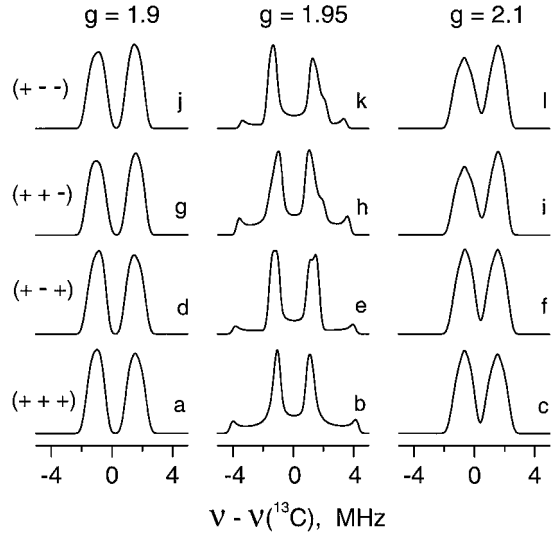

FIG. 4. ^{13}C ENDOR spectra (35 GHz) simulated using hyperfine tensor parameters presented in Table 2 for positive A_{xy}, A_{xz}, and A_{yz}. All linewidths are the same as in Fig. 1.

and 5. Comparison of Fig. 3 with Figs. 4 and 5 shows a best fit for $(+ + -)$ signs of A_{xx}, A_{yy}, and A_{zz} elements, and for positive nondiagonal elements, in accordance with the $\boldsymbol{A}_{exact}$. That is also confirmed by the principal values and Euler angles given in Table 2 (note also that for set **II** the $(+ - -)$ signs of A_{xx}, A_{yy}, and A_{zz} elements and positive nondiagonal elements also give satisfactory agreement with the "observed" spectra).

The two cases considered demonstrate that procedure proposed allows rapid and accurate determination of the principal elements of hyperfine tensor, and its orientation in the g-tensor coordinate system, over a broad range of relative values of hyperfine and nuclear Zeeman interactions. One can conclude also that the accuracy of the method is higher when hyperfine interaction is comparable with the nuclear Zeeman interaction.

The procedure has also been tested using several sets of published experimental ENDOR data. Application of our treatment to ENDOR experimental spectra gives tensor components, relative to those obtained after numerical simulations of spectra at canonical and other intermediate orientations, with accuracy similar to that obtained with the model examples above. The procedure can definitely be used as a first step in the analysis of the orientation-selected spectra. This test shows that the accuracy of the procedure is directly associated with the accuracy in the determination of the nuclear frequencies. In this respect one can suggest that it will give increasingly better results for experimental data obtained at high microwave frequencies (Q- and W-band

TABLE 2

Different Sets of Hyperfine Interaction Parameters Determined from Spectra (Fig. 3) Simulated with $A_1 = -6$ MHz, $A_2 = 2$ MHz, $A_3 = 8$ MHz, $\alpha = 30°, \beta = 60°, \gamma = 165°$

The sign of A_{xx}, A_{yy}, and A_{zz}	A_1, MHz	A_2, MHz	A_3, MHz	α, ○	β, ○	γ, ○
$(+ + +)^a$	−3.58	2.03	9.23	29.2	48.2	173.3
$(+ - +)^a$	−4.55	−1.99	8.80	17.2	46.6	32.8
$(+ + -)^a$	−6.29	2.00	7.65	30.4	57.2	174.9
$(+ - -)^a$	−6.75	−2.41	7.11	15.8	56.0	16.7
$(+ + +)^b$	−4.24	3.41	8.51	197.8	45.2	8.4
$(+ - +)^b$	−5.62	−0.50	8.38	188.9	45.6	36.3
$(+ + -)^b$	−6.74	3.35	6.74	194.0	55.0	8.35
$(+ - -)^b$	−7.51	−1.20	6.65	185.5	55.8	26.8

[a] Positive A_{xy}, A_{xz}, and A_{yz}.
[b] Negative A_{xy}, A_{xz}, and A_{yz}.

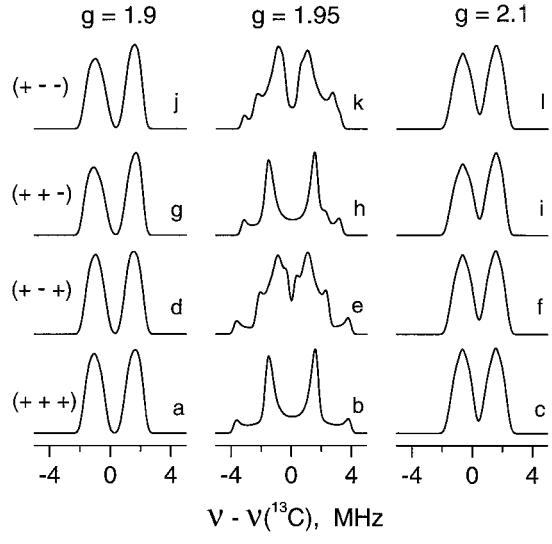

FIG. 5. ^{13}C ENDOR spectra (35 GHz) simulated using hyperfine tensor parameters presented in Table 2 for negative A_{xy}, A_{xz}, and A_{yz}. All linewidths are the same as in Fig. 1.

and higher) (*9, 17–19*), where the selected range of orientations is significantly smaller due to a larger spread of the EPR powder pattern, and where the measured ENDOR/ESEEM spectra better approach the condition "single-crystal-like." It can also be applicable for nuclei with $I \geq 1$ if the quadrupole splittings are small and not resolved in the orientation-selected spectra.

ACKNOWLEDGMENTS

This work was supported by NATO Grant PST.EV.976506 and NIH Grant R01 RR01811-15 to the Illinois EPR Research Center. A.S. thanks NATO for the support of his sojourn at the University of Illinois and Illinois EPR Research Center for the hospitality.

REFERENCES

1. A. J. Hoff, Ed., "Advanced EPR. Applications in Biology and Biochemistry," Elsevier, Amsterdam (1989).

2. B. M. Hoffman, V. J. DeRose, P. E. Doan, R. J. Gurbiel, A. L. P. Houseman, and J. Telser, Metalloenzyme active-site structure and function through multifrequency CW and pulsed ENDOR, *Biol. Magn. Reson.* **13,** 151–218 (1993).

3. J. Hüttermann, ENDOR of randomly oriented mononuclear metalloprotein: Toward structural determination of the prosthetic group, *Biol. Magn. Reson.* **13,** 219–252 (1993).

4. S. A. Dikanov and Yu. D. Tsvetkov, "Electron Spin Echo Envelope Modulation (ESEEM) Spectroscopy," Boca Raton, FL (1992).

5. Y. Deligiannakis, M. Louloudi, and N. Hadjiliadis, Electron spin echo envelope modulation (ESEEM) spectroscopy as a tool to investigate the coordination environment of metal centers, *Coord. Chem. Rev.* **204,** 1–112 (2000).

6. R. H. Rist and J. S. Hyde, Ligand ENDOR of metal complexes in powders, *J. Chem. Phys.* **52,** 4633–4643 (1970).

7. B. M. Hoffman, J. Martinsen, and R. A. Venters, General theory of polycrystalline ENDOR patterns: *g* and *A* hyperfine tensors of arbitrary symmetry and relative orientation, *J. Magn. Reson.* **59,** 110–123 (1984).

8. P. E. Doan and B. M. Hoffman, Simulating 2-D, [Field-Frequency], orientation-selective ENDOR and ESEEM patterns, *EPR Newsl.* **10**(3), 10–14 (1999).

9. H.-I. Lee, L. M. Cameron, B. J. Hales, and B. M. Hoffman, CO binding to the FeMo cofactor of CO-inhibited nitrogenase: ^{13}CO and ^{1}H *Q*-band ENDOR investigation, *J. Am. Chem. Soc.* **119,** 10,121–10,126 (1997).

10. R. Kappl, S. Ciurli, C. Luchinat, and J. Hüttermann, Probing structural and electronic properties of oxidized $[Fe_4S_4]^{3+}$ cluster of *Ectothiohordospira halophila* iso-II high-potential iron–sulfur protein by ENDOR spectroscopy, *J. Am. Chem. Soc.* **121,** 1925–1936 (1999).

11. H. M. McConnell, A pseudovector nuclear hyperfine interaction, *Proc. Natl. Acad. Sci. U.S.A.* **44,** 766 (1958).

12. F. K. Kneubühl, Symmetrie und Mikrowellen Spektren mehratomiger paramagnetischer Zentren, *Phys. Kondens. Mater.* **1,** 410–447 (1963).

13. F. K. Kneubühl, Paramagnetische Resonanz von Zentren mit den Symmetrien $n, \bar{n}$ und n/m, *Phys. Kondens. Mater.* **4,** 50–62 (1965).

14. A. Schweiger, "Electron Nuclear Double Resonance of Transition Metal Complexes with Organic Ligands," Structure and Bonding, Vol. 51, Springer-Verlag, Berlin (1982).

15. J. R. Pilbrow and M. R. Lowrey, Low-symmetry effects in electron paramagnetic resonance, *Rep. Prog. Phys.* **43,** 433–495 (1980).

16. B. M. Hoffman, R. A. Venters, and J. Martinsen, General theory of polycrystalline ENDOR patterns. Effects of finite EPR and ENDOR component linewidths, *J. Magn. Reson.* **62,** 537–542 (1985).

17. H.-I. Lee, M. Sørlie, J. Christiansen, R. Song, D. R. Dean, B. J. Hales, and B. M. Hoffman, Characterization of an intermediate in the reduction of the acetylene by the nitrogenase α-Gln ^{195}MoFE protein by Q-band EPR and ^{13}C, ^{1}H ENDOR, *J. Am. Chem. Soc.* **122,** 5582–5587 (2000).

18. P. Manikandan, R. Carmieli, T. Shane, A. J. Kalb (Gilboa), and D. Goldfarb, W-Band ENDOR investigation of the manganese-binding site of Concanavalin A: Determination of proton hyperfine couplings and their signs, *J. Am. Chem. Soc.* **122,** 3488–3494 (2000).

19. G. Bar, M. Bennati, H.-H. T. Nguyen, J. Ge, J. Stubbe, and R. G. Griffin, High-frequency (140 GHz) time domain EPR and ENDOR spectroscopy: The tyrosyl radical–diiron cofactor in ribonucleotide reductase from yeast, *J. Am. Chem. Soc.* **123,** 3569–3576 (2001).